Frozen and active regions in diffusion-limited aggregation clusters

Hervé Boularot and Gilbert Albinet
Institut de Recherche Sur les Phénomènes Hors Équilibre, CNRS UMR No. 138, Université de Provence, Centre Saint-Jérôme, Case 252, 13397 Marseille, France
(Received 17 July 1995)

This paper is devoted to the study of the properties of the diffusion-limited aggregation (DLA) and diffusion-limited deposition (DLD) clusters, both in the frozen and in the active zones. First, we show that the angular distribution in the frozen zone of a DLA aggregate, defined from the normalized distance between branches, obeys a ''multifractal'' statistics: this result is compared to the hole size distribution in the triadic Cantor set (discontinuous distribution). Second, our interest focuses on the tip effect in the external active zone. Measures concern the evolution of the condensation height as well as the position of the free particles diffusing in the fjords versus the distance to the tips. In both cases, the laws obtained depend on one parameter only, α_s and α_p in the DLD case, α_s' and α_p' for DLA clusters. [S1063-651X(96)04305-X]

PACS number(s): 68.70.+w, 05.40.+j, 64.60.Cn

I. INTRODUCTION

The fractal structures [1] generated by the diffusion-limited aggregation (DLA) method proposed by Witten and Sander [2] are representative of a great variety of physical clusters [3–7]. Schematically, two regions can be distinguished in such aggregates (Fig. 1): the internal frozen zone where the free particles never come, and an external active zone where new particles stick. The sticking probability distribution $p(i)$, associated to each site labeled i in contact with the growing cluster, is multifractal [8].

In the first section of this paper, the frozen zone of small on-lattice DLA clusters is statistically analyzed: each cluster contains 10^4 particles and, for such a scale, on-lattice and off-lattice clusters do not present noticeable differences [9]. In this zone, the relevant parameter is not the condensation probability on each cluster site [8] (the diffusing particles cannot visit this region) but another set of probabilities corresponding to the sizes of the empty spaces between branches. This set of probabilities is equivalent to an angular distribution. Using the fact that the dimension of an azimuthal section of the DLA cluster is close to the Cantor set dimension (ln2/ln3), this angular distribution is compared to the normalized hole size distribution associated to the triadic Cantor set.

In the second part, we consider the active zone and the tip effect is quantitatively evaluated for DLA and diffusion-limited deposition (DLD). The evolution of two representative variables, related to the tip effect, is measured versus the distance to the tip: $r_{\max}-r$ or $h_{\max}-h$: the condensation rate on the cluster, R_c, and the penetration rate into the fjords, R_p. R_c is compared to the sticking probability defined in [10].

II. ''MULTIFRACTAL'' PROPERTIES OF THE FROZEN ZONE

A. Cantor set

The intersection between the frozen zone of DLA aggregates and circles of radius r, centered on the original seed, will be compared to the triadic Cantor set. The normalized hole size distribution of the latter set is studied first (Fig. 2). The qth-order moments $M(q,N)$, at the Nth iteration of the fractal set, are defined by

$$M(q,N)=\sum_{j=1}^{N_H} p(j,N)^q, \quad \text{with } N_H=2^N-1$$

$$\text{and } p(j,N)=l_{\text{arc}}(j,N)/\lambda(N), \tag{1}$$

where N_H represents the number of holes, $l_{\text{arc}}(j,N)$ is the length of the jth empty hole, $\lambda(N)=3^N-2^N$ is the total hole length (3^N is the set length at step N), and $p(j,N)$ is the probability associated to the jth hole at the step N.

We use here the classical notations for a ''multifractal'' analysis to describe this well-known pure fractal set, i.e., the exponent τ_q which represents the self-similar behavior of the q-order moments:

$$M(q,N)=\varepsilon^{\tau_q} \quad \text{with } \varepsilon=3^{-N}. \tag{2a}$$

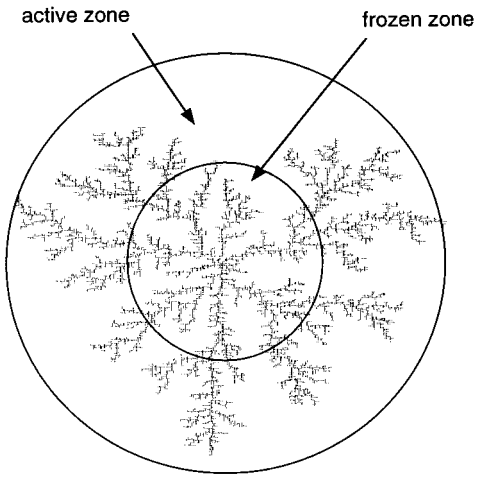

FIG. 1. Active and frozen zones of a DLA cluster.

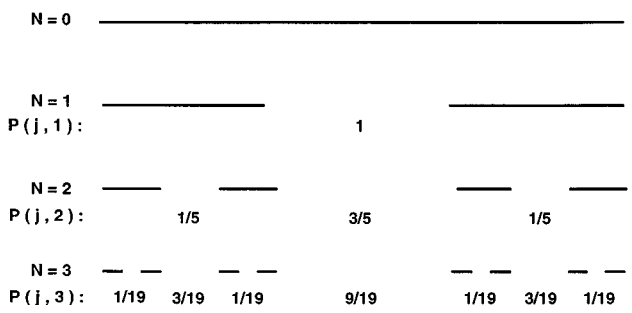

FIG. 2. Normalized hole size distribution associated with three iterations of a triadic Cantor set.

Applying the classical Legendre transform to q and τ_q, we obtain the exponents α and $f(\alpha)$ [8,11,12]:

$$\alpha(q)=d\tau_q/dq, \quad f(\alpha)=q\alpha-\tau_q. \tag{2b}$$

The analytical expressions of these functions can be easily obtained in the self-similar limit $N\to\infty$: In the large scale domain, for $q>q_0$, $q_0=\ln 2/\ln 3$,

$$\tau_q=0, \quad \alpha(q)=0, \text{ and } f(\alpha)=0, \tag{3a}$$

in the small scale domain, for $q<q_0$,

$$\tau_q=q-q_0, \quad \alpha(q)=1, \text{ and } f(\alpha)=q_0. \tag{3b}$$

It is easy to understand why the $f(\alpha)$ function is limited to two points only. The exponents α and $f(\alpha)$ are, respectively, associated with the probability distribution $p(\epsilon)$ of the hole sizes at the Nth iteration step, and with the corresponding hole number N_{eff}: $p(\varepsilon)\approx\varepsilon^{\alpha}$ and $N_{\text{eff}}\approx\varepsilon^{-f(\alpha)}$. In the Cantor case $p=3^{-\alpha N}$ and $N_{\text{eff}}=3^{f(\alpha)(N-1)}$.

For scales larger than ϵ, i.e., at an iteration step $n<N$, in the limit $N\to\infty$, the statistical weight p of the holes created at the nth iteration of the Cantor set is independent of N and converges towards the constant value 3^{-n} when N converges towards infinity. On the other hand, the number of these holes of size 3^{-n} remains unchanged when N increases. These two conditions imply that α and f are equal to zero in the limit $q<q_0$.

For the smallest scale $p\approx 3^{-N}$ implies $\alpha=1$. At each iteration step, the number of smallest holes is multiplied by a factor 2 and their size is divided by a factor 3; then $f=\ln 2/\ln 3$.

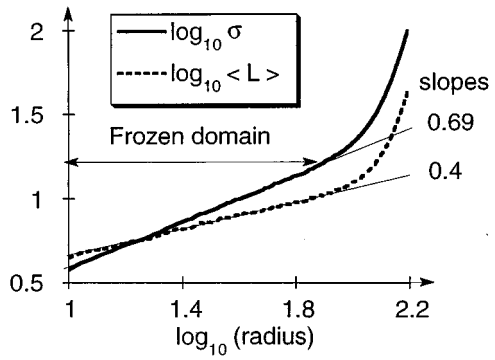

FIG. 3. Radius dependency of the mean hole size and standard deviation for DLA aggregates.

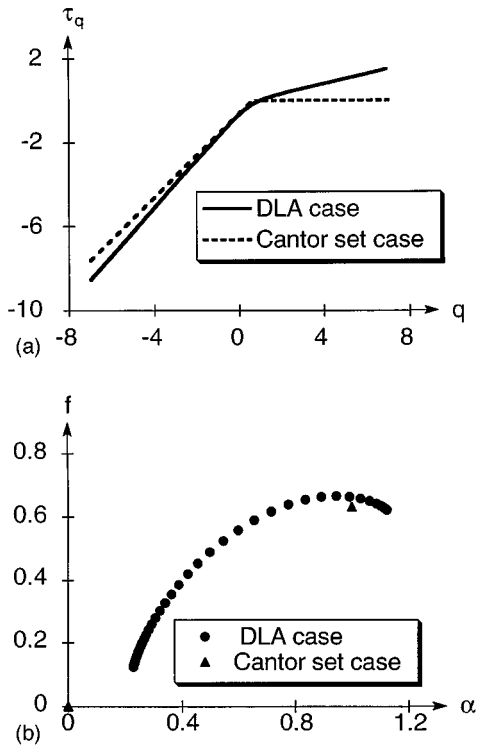

FIG. 4. (a) τ_q versus q diagrams for $q\in[-7,7]$ representative of the angular distribution in the frozen zone of DLA clusters and of the normalized hole size distribution in the Cantor set case. (b) $f(\alpha)$ versus $\alpha(q)$ curves for the Cantor set and the DLA clusters.

B. DLA clusters

We study the angular distribution in the frozen zone of DLA aggregates. 10^3 clusters containing 10^4 particles are necessary to obtain accurate results. First, the evolution of the arc mean length and the standard deviation σ are measured when r increases. The moments $\langle L(q,r)\rangle$ and σ are defined as follows ($\langle L(1,r)\rangle$ is the arc mean length):

$$\langle L(q,r)\rangle=\frac{1}{N_1}\sum_{i=1}^{N_1}\frac{1}{N_2(i,r)}\sum_{j=1}^{N_2(i,r)} l_{\text{arc}}(j,r)^q, \tag{4a}$$

$$\sigma(r)=[\langle L(2,r)\rangle-\langle L(1,r)\rangle^2]^{1/2}. \tag{4b}$$

N_1 is the number of aggregates and N_2 is the number of branches (or the number of holes) of the ith cluster at a given radius r. l_{arc} is the length of the jth azimuthal section, in the ith cluster, at a given radius r.

A self-similar behavior, corresponding to the frozen zone, is clearly obtained in Fig. 3, over about one decade, between $r=20$ and 200. This result shows that clusters containing 10^4 particles are sufficient to display scaling laws. The exponents associated with $\langle L(1,r)\rangle$ and σ are, respectively, $\beta_1=0.4\pm0.02$ ($\cong 2-D_f$) and $\beta_\sigma=0.69\pm0.02$. This last exponent is representative of a wide length scale distribution.

We also compute the moments $M(q,r)$, defined as follows:

$$M(q,r)=\frac{1}{N_1}\sum_{i=1}^{N_1}\sum_{j=1}^{N_2(i,r)} p(j,r)^q=\varepsilon^{\tau_q}, \tag{5}$$

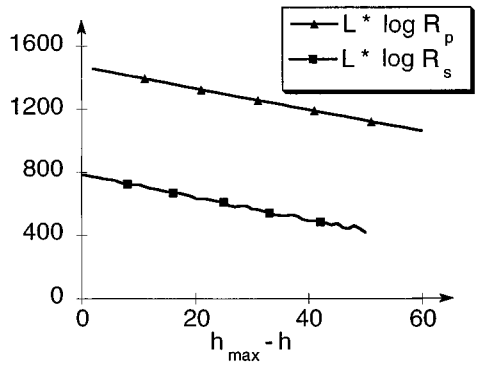

FIG. 5. Sticking rate (slope: $\alpha_s \cong 7.2$) and penetration rate (slope: $\alpha_p \cong 6.8$) for the DLD clusters.

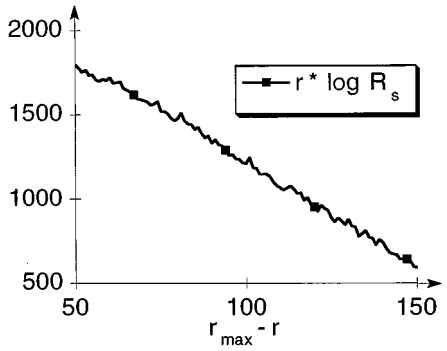

FIG. 6. Sticking rate (slope: $\alpha_s' \cong 10$) for the DLA clusters.

with $p(j,r)=l_{\text{arc}}(j,r)/\lambda(r)$ and $\varepsilon=1/r$ in the DLA case, $\lambda(r)$ being the total hole length at a radius r. The moments $M(q,r)$ are equivalent to the analytically calculated moments of the Cantor set $M(q,N)$.

Respectively, Figs. 4(a) and 4(b) represent the behaviors of the exponents τ_q (for q varying from -7 to 7, by 0.1 steps), and $f(\alpha)$ versus $\alpha(q)$; they are compared with the Cantor set results plotted in the same figures. This approach provides useful results about the angular distributions in DLA clusters.

In the two linear regions of the τ_q curves the angular distribution presents a simple fractal structure, i.e., we can define a gap exponent Δ, allowing us to deduce τ_q from τ_{q-1} by the linear relation $\tau_q=\tau_{q-1}+\Delta$. Δ is similar to the gap scaling presented by critical phenomena where it is given by successive derivatives of the free energy.

The negative values of q ($q \in]-\infty,-0.4]$ and in the simulation -7 is identified with $-\infty$) enhance the contribution of unlikely regions (small arcs) corresponding to the most acute angles: the linear curve τ_q versus q is linear with a gap exponent, $\Delta_{-\infty}=\alpha_{-\infty} \cong 1.15$, close to the Cantor set value ($\Delta_{-\infty}=1$). This exponent is simply characteristic of the branching condition when the cluster size increases: the arc length of the smallest holes being independent of the radius, the associated probability is proportional to $\varepsilon=1/r$, which leads to $\alpha_{-\infty}=1$.

A major difference between the Cantor set and the DLA clusters appears in the large q domain, here $q>1.6$. The largest angular sector contribution decreases with the radius: $p \approx r^{-\Delta_{+\infty}}$, with $\Delta_{+\infty}=\alpha_{+\infty} \cong 0.24$ (in the Cantor set case, p remains constant: $\Delta_{+\infty}=\alpha_{+\infty}=0$).

In the simulation results, the nonlinear region of τ_q is limited to a narrow interval of q: Δq ($q \in [-0.4,1.6]$, $\Delta q \cong 2$). Δq gives information on the angular distribution of the fractal sets. From the various articles devoted to the multifractal analysis (see, for example, [8,11,12]), it appears that Δq and the probability distribution spreading are related as follows: to a wide angular distribution corresponds a small value for Δq. In our case, one can consider that Δq is small (equivalent to a wide distribution) in comparison with the transition domains of the multifractal sets displayed in [8,12]. The Cantor set is representative of a limiting case where Δq does not exist: the probabilities associated with the holes created at a given iteration of the fractal set tend to a constant value under iterations. This is not the case for the sets displayed in [8,11,12] and for our DLA aggregates: all the probabilities obey power laws and tend to zero in the fractal limit. This measure allows us to differentiate various sets of the same fractal dimension.

III. TIP EFFECT IN DLA AND DLD CLUSTERS

This section is devoted to the statistical measure of the tip effect in the active zone of the DLD and of the DLA clusters. Two parameters representative of this effect can be defined: the sticking rate onto the aggregate, R_s, and the penetration rate into the fjords, R_p. R_s and R_p are computed as follows. For each cluster built, a given number of particles, N, are launched one by one. The condensation height and the position at each diffusing step in the lacuna are, respectively, recorded in R_s and R_p. After condensation, each particle is removed in order to keep the cluster unchanged. R_s and R_p depend on the distance to the tip, $h_{\max}-h$ (DLD case) or $r_{\max}-r$ (DLA case). By definition, $h_{\max}$ and $r_{\max}$ represent the tip of the smallest cluster given by the statistic. These simulations are done over 1000 clusters containing 8000 and 10^4 particles in the DLD and the DLA cases, respectively. In Figs. 5 and 6, R_s and R_p are obtained by addition and removing of 1000 particles to each aggregate: so the sample is done over $10^3 \times 10^3$ additional particles. In our figures, only the domains located below the limit $h_{\max}$ and $r_{\max}$ are considered. The measures performed in the DLD case, for the two sample sizes $L=50$ and 100, lead to the following exponential laws (Fig. 5):

$$R_s \approx \exp[-\alpha_s(h_{\max}-h)/L], \tag{6a}$$

$$R_p \approx \exp[-\alpha_p(h_{\max}-h)/L], \tag{6b}$$

with $\alpha_s \cong 7.2$, close to $\alpha_p \cong 6.8$, L being the characteristic length.

For DLA aggregates, the decreasing laws take a more complicated form (Figs. 6 and 7). For this last figure, the statistics are done over 40 aggregates (4×10^4 additional particles only) of different sizes:

$$R_s \approx \exp[-\alpha_s'(r_{\max}-r)/r], \tag{7a}$$

$$R_p \approx \exp[-\alpha_p'(r_{\max}-r)/r], \tag{7b}$$

with $\alpha_s' \cong 10$ and $\alpha_p' \cong 21$.

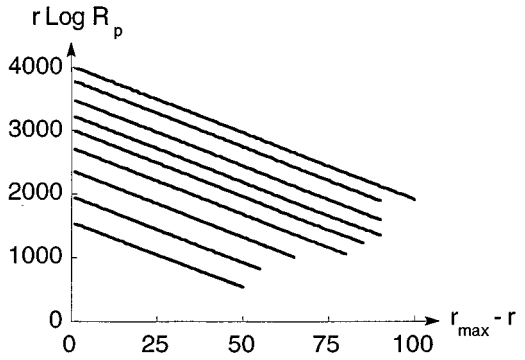

FIG. 7. Penetration rate (slope: $\alpha_p' \cong 21$) in DLA aggregates for nine different cluster sizes, N_c: each curve corresponds to a given value of N_c, varying from 4000 (the lowest curve) to 20 000 (the highest curve), by step of 2000 particles. We only represent the region situated near the tips, corresponding to a large sample.

It is interesting to compare these results to the previous works concerning the active zone of the DLA clusters and, more specifically, to compare R_s to the sticking probability $P(r,N_c)$, where N_c represents the number of particles in a DLA cluster. A Gaussian law, obtained by an average over the total number of additional particles, was found by Plischke and Racz [10] to represent the sticking probability. This distribution is centered on the radius $r'_{\max}$, associated with the maximum of the condensation probability. The behaviors, in the $r > r'_{\max}$ and the $r < r'_{\max}$ domains, are, respectively, associated with the decrease of the branch number and with the tip effect. Their measures of the standard deviation associated to $P(r,N_c)$ lead to the relationship $\sigma \approx N_c^{\nu}$ with $\nu \cong 0.48$. Remaining in the Gaussian law hypothesis, subsequent extensive simulations have shown that the exponent ν depends on N_c ($\nu \to 1/D_f$ in the limit $N_c \to \infty$) [13] and that other corrections must be added to the standard deviation [14]. In spite of these simulations, the asymptotic behavior of the active region is still unclear [15]. Owing to our definition of $r_{\max}$, the statistics associated with R_s (Fig. 6) corresponds to the domain $r < r_{\max} < r'_{\max}$ of $P(r,N_c)$. The tip effect, included in $P(r,N_c)$, is characterized by Eqs. (1) and (2): these relations throw back into question the Gaussian law proposed in [10].

Some remarks can be made about these relations. For the deposition problem, R_p and R_s both obey an exponential law of same slopes α, $\alpha = \alpha_s \cong \alpha_p$; for the DLA problem, two laws of same form are obtained for R_p and R_s with two different slopes: $\alpha_s' < \alpha_p'$. As for the deposition and for the aggregation problem, relations (1) and (2) imply that there is a large correlation between the paths in the lacunas, characterized by R_p, and the sticking heights, characterized by R_s. The path followed by a diffusing particle in the fjords represent the history of the condensation process which explain the correlations obtained between R_p and R_s.

A comparison between the decreasing of the number of condensation sites, N_s (related to R_s), and the number of fjord sites, N_H (related to R_p), versus the distance to the tip can qualitatively explain the two relations: $\alpha_s \cong \alpha_p$ and $\alpha_s' < \alpha_p'$. For the DLA aggregates, the polar geometry implies that N_s and N_H are, respectively, proportional to $r^{D_f - 1}$ and r. These two power laws imply that N_H decreases faster than N_s during the penetration process, then R_p decreases faster than R_s, which involves $\alpha_s' < \alpha_p'$. For the deposition clusters the preceding effect coming from the polar geometry of a DLA cluster does not exist: the sum $N_s + N_H + N_a$ is equal to a constant: L ($= 2\pi r$ in the DLA case, N_a represents the number of aggregate sites). However, the number of fjord and sticking sites weakly depends on $(h_{\max} - h)$ because the measurements are made on the lower part of the active zone. Then, we can consider that $\alpha_s \cong \alpha_p$ and $R_p \approx R_s$.

From a numerical point of view, the penetration parameters are measured with higher precision than the condensation one (see Figs. 5–7): the sampling is done over the sticking sites only in the condensation case and over all the sites visited by diffusion in the penetration case.

Another interesting question concerns the N_c dependency on the α_s', α_p', and α parameters. In the deposition problem, the statistics displayed in Fig. 5 is figured far from the seed. In this domain, the tip of the cluster and thus α remain unchanged when N_c (or h) increases. On the other hand, a statistical analysis is necessary to measure the N_c dependency of the two slopes associated to the DLA aggregates. The penetration rate is displayed in Fig. 7 for nine cluster sizes (40 aggregate of each size): N_c varies between 4×10^3 and 2×10^4 particles by 2×10^3 step. A sample of 4×10^4 additional particles is used for each cluster size (this sample is sufficient to obtain accurate slopes for R_p). From this last simulation, it appears clearly that α_p' does not depend on N_c. The statistics associated with α_s' and not shown here provides the same results. The linear domains displayed in Figs. 5–7 are in fact independent of an $h_{\max}$ or an $r_{\max}$ translation. From this last part, we can conclude that the tip effect is characterized by the parameters α in the DLD case, α_p' and α_s' for DLA aggregates.

IV. CONCLUSION

The first part of this article was devoted to the study of the inner regions of the DLA aggregates and particularly to the comparison between the triadic Cantor set ($D_f = \ln 2/\ln 3 \cong 0.63$) and the azimuthal cut of the frozen regions of the DLA clusters ($D_f \cong 0.65$). The ''multifractal'' analysis associated with the angle distribution (DLA) and with the normalized hole size distribution (Cantor set) were performed in order to reveal the differences between these two sets which have roughly the same fractal dimension: In the DLA (Cantor set) case, an angle (hole) is associated with each cluster site (to each occupied segment). The major differences between these two distributions come from the large angle (hole) contributions: for the DLA aggregates (Cantor set), the probabilities associated with the largest angles (the largest holes) obey a power law and tend to zero (to nonzero constants) in the fractal limit. In a general way, the method presented in this article could be applied to numerous fractal aggregates such as the polymers, in the limit $r < R_g$ (gyration radius), the percolation clusters near threshold, or the crystal growth aggregates, for example. In the second part, two general laws (for the DLA and the DLD aggregates) representative of the tip effect were obtained both in the penetration and in the sticking cases. Moreover, the simulations have

shown that the parameters α, α_p', and α_s', are independent of the cluster sizes. Each of these laws is characterized by one parameter only. Finally, it is interesting to note that these laws are also obtained for anisotropic ramified clusters [16].

ACKNOWLEDGMENTS

We are very pleased to thank J.-M. Debierre and R. Julien for useful discussions.

[1] B. B. Mandelbrot, *The Fractal Geometry of Nature* (Freeman, New York, 1982).
[2] T. A. Witten and L. M. Sander, Phys. Rev. Lett. **47**, 1400 (1981); Phys. Rev. B **27**, 5686 (1983).
[3] G. Radnoczy, T. Vicsek, L. M. Sander, and D. Grier, Phys. Rev. A **35**, 4012 (1987).
[4] L. Niemeyer, L. Pietronero, and H. J. Wiesmann, Phys. Rev. Lett. **52**, 1033 (1984).
[5] M. Matsushita, M. Sano, Y. Hayakawa, H. Honjo, and Y. Sawada, Phys. Rev. Lett. **53**, 286 (1984).
[6] Y. Couder, O. Cardoso, D. Dupuy, P. Tavernier, and W. Thom, Europhys. Lett. **2**, 437 (1986).
[7] A. Kuhn, F. Argoul, J. F. Muzy, and A. Arneodo, Phys. Rev. Lett. **73**, 2998 (1994).
[8] Y. Hayakawa, S. Sato, and M. Matsushita, Phys. Rev. A **36**, 1963 (1987).
[9] T. Vicsek, *Fractal Growth Phenomena*, 2nd ed. (World Scientific, Singapore, 1992).
[10] M. Plischke and Z. Racz, Phys. Rev. Lett. **54**, 861 (1985).
[11] T. C. Halsey, M. H. Jensen, L. P. Kadanoff, I. Procaccia, and B. I. Schraiman, Phys. Rev. A **33**, 1141 (1986).
[12] E. Stanley and P. Meakin, Nature (London) **335**, 405 (1988).
[13] P. Meakin and L. M. Sanders, Phys. Rev. Lett. **54**, 2053 (1985).
[14] P. Ossadnik, Physica A **195**, 319 (1993).
[15] B. B. Mandelbrot, H. Kaufman, A. Vespignani, I. Yekutieli, and C.-H. Lam, Europhys. Lett. **29**, 599 (1995).
[16] H. Boularot, Ph.D. thesis, Aix-Marseille I, 1995.